Topological charge Fano effect in multi-Weyl semimetals

W. C. Silva,[1] W. N. Mizobata,[1] J. E. Sanches,[1] L. S. Ricco,[2] I. A. Shelykh,[2,3] M. de Souza,[4] M. S. Figueira,[5] E. Vernek,[6] and A. C. Seridonio[1,*]

[1]*São Paulo State University (Unesp), School of Engineering, Department of Physics and Chemistry, 15385-000 Ilha Solteira-SP, Brazil*

[2]*Science Institute, University of Iceland, Dunhagi-3, IS-107 Reykjavik, Iceland*

[3]*ITMO University, St. Petersburg 197101, Russia*

[4]*São Paulo State University (Unesp), IGCE, Department of Physics, 13506-970 Rio Claro-SP, Brazil*

[5]*Instituto de Física, Universidade Federal Fluminense, 24210-340 Niterói, Rio de Janeiro, Brazil*

[6]*Instituto de Física, Universidade Federal de Uberlândia, Uberlândia, 38400-902 Minas Gerais, Brazil*

(Received 28 March 2022; revised 11 June 2022; accepted 13 June 2022; published 24 June 2022)

We theoretically analyze the Fano interference in a single impurity multi-Weyl semimetal hybrid system and show the emergence of the topological charge Fano effect in the bulk local density of states. In multi-Weyl semimetals, the number of Fermi arcs at the system boundaries is determined by the topological charge J, a direct consequence of the "bulk-boundary" correspondence principle. Analogously, we find that J also modulates the bulk Fano profile of the system with an embedded quantum impurity. Thus by increasing J, the Fano line shape evolves from resonant, typical for $J = 1$ (single Weyl), towards antiresonant, extrapolating to the so-called hyper Weyl semimetals with $J \gg 1$. Specially for the maximum case protected by the rotational symmetry $C_{2J=6}$, namely, the $J = 3$ (triple Weyl), which acquires asymmetric Fano profile, the Fano parameter absolute value is predicted to be $\tan(C_{2J=6})$, where $C_{2J} \equiv (360^\circ/2J)$ defines the rotational angle. Hence, the Fano discretization in the J term introduces the topological charge Fano effect in multi-Weyl semimetals. We also suggest a transport device where we expect that the proposed Fano effect could be detected.

DOI: 10.1103/PhysRevB.105.235135

I. INTRODUCTION

Multi-Weyl semimetals [1–8] are intriguing generalizations of standard Weyl semimetals [9–19], once they can lead to a plethora of fascinating effects, such as chiral, optical and transport anomalous properties [7–9,11,16–18,20–22]. In multi-Weyl semimetals, the band-structures at the so-called Weyl crossing points, show highly anisotropic dispersion relations, being relativistic exclusively in one momentum direction, while in the other two, a power-law dependence is ruled by the topological charge J [19]. This topological number corresponds to the quantized Berry phase of the Dirac fermions in graphene [23]. As Weyl points appear in pairs with opposite chiralities, they behave as source and drain of an Abelian Berry curvature, thus mimicking (anti)monopoles placed far apart in the reciprocal space. Amazingly, such points are connected to each other via crystal boundaries, in particular, by opened surface states known as Fermi arcs. Notably, these exotic states can be observed by ARPES [1,2] and turn into the experimental proof of the magnetic monopoles existence in the momenta space.

In multi-Weyl semimetals, the winding number also plays the role of a higher topological charge $J > 1$ [1]. This charge arises from the merging of J single chiral-degenerate Weyl nodes into multi-Weyl points, which are point group symmetry protected up to $J = 3$ [15], namely, by means of the rotational symmetry C_{2J}. In this manner, the "bulk-boundary" correspondence dictates that for a given J value determined in an infinite bulk system, J pairs of Fermi arcs appear in the corresponding finite version of the setup [10]. Some examples of multi-Weyl materials are $HgCr_2Se_4$ and $SrSi_2$ with $J = 2$ (double Weyl) [12,15,20,24], and $A(MoX)_3$ (A=Rb or Tl and X=Te) with $J = 3$ (triple Weyl) [13].

In this work, we focus on the "bulk-boundary" correspondence for Fermi arcs surface states and the topological charge from the bulk, in order to present the concept of the topological charge Fano effect in multi-Weyl semimetals. To this end, we theoretically explore the bulk Fano interference [25,26] in the LDOS (*local density of states*) for a single impurity multi-Weyl semimetal hybrid system, as sketched in Fig. 1(a). As a matter of fact, the Fano interference arises from the coupling between a discrete energy level and an energy continuum [26]. It has been widely investigated in several platforms, ranging from classical mechanics [27] to topological superconductivity [28,29]. Coupled harmonic oscillators with a driving force [27], photonic systems [30], Jaynes-Cummings-like cavities [31], electronic quantum transport setups made of Anderson adatoms [32–35], atomically frustrated molecules in Weyl metals [8], and topological superconducting nanowires with quantum dots [29], among others [26], constitute the broad variety of examples where Fano interference manifests itself.

Here, we reveal that the increase of J modifies the bulk Fano profile of a multi-Weyl semimetal with a single impurity, by means of the tuning of Fano asymmetry parameter q_J, from resonant line shape ($|q_{J=1}| \to \infty$) towards antiresonant one ($|q_{J\gg1}| \to 0$). We highlight that while the former

*Corresponding author: antonio.seridonio@unesp.br

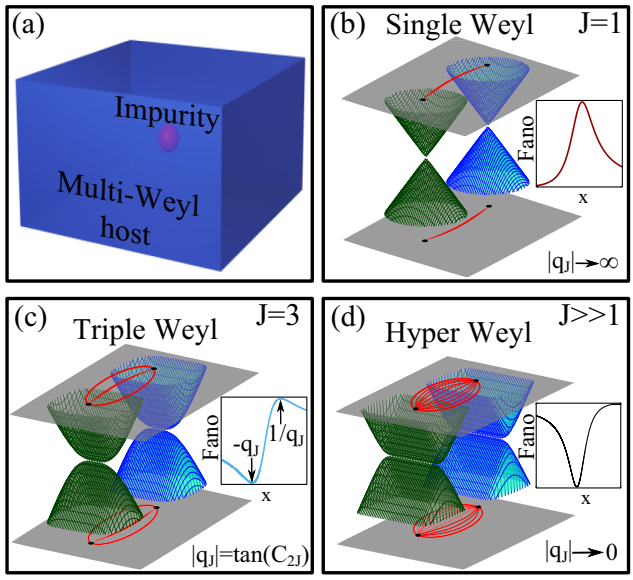

FIG. 1. Overview of the topological charge Fano effect in multi-Weyl semimetals. (a) Slab of a bulk multi-Weyl semimetal system hosting an impurity. [(b)–(d)] Qualitative summary of our findings: corresponding band structures from Eq. (3) with $k_y = 0$, $Q = 0.4k_D$ and Fermi arcs surface states upon changing the topological charge J. Related bulk Fano profiles vs the dimensionless resonant energy detuning x of the impurity appear depicted at the inset panels. The Fano profile evolves from resonant behavior (b) to the antiresonant-type (d) as J increases. The pairs of Fermi arcs are determined by the J value, which imposes the bulk Fano line shape. This profile is determined by the absolute value of the Fano asymmetry parameter $|q_J| = \tan(C_{2J})$ (c), where $C_{2J} \equiv (360^\circ/2J)$ stands for the angle of the rotational symmetry group. In summary, the "bulk-boundary" correspondence [10] defines the grounds of the topological charge Fano effect in multi-Weyl systems.

identifies $J = 1$ case (single Weyl) [inset panel of Fig. 1(b)], the latter predicts a Fano antiresonant profile characterized by $J \gg 1$. For such a case, we relax, as we shall clarify later on, the aforementioned crystalline protection [15] and make explicit that the fingerprint for this situation, which we introduce as the hyper Weyl semimetal, is represented by a suppressed Fano parameter ($|q_{J\gg1}| \to 0$) [inset panel of Fig. 1(d)].

We clarify that hyper Weyl semimetals should be understood as a conjecture, being a hypothetical case corresponding to a huge topological charge. However, some research groups have reported spinless platforms with $J = 4$ [36,37], pointing out that it is still capital to consider a generalized description. Noteworthy, for $J \geqslant 3$, the Fano parameter becomes finite, discretized in J and shows a decaying behavior. Particularly for the maximum allowed case by the point symmetry group protection, i.e., the $J = 3$ value for the $C_{2J=6}$ rotational symmetry group, we predict $|q_{J=3}| = \tan(C_{2J=6})$, with the rotational angle $C_{2J} \equiv (360^\circ/2J)$ and an asymmetric Fano line shape [inset panel of Fig. 1(c)]. Thereby, our findings introduce the idea of the topological charge Fano effect in multi-Weyl semimetals.

II. THE MODEL

The Hamiltonian mimicking our system [Fig. 1(a)], with $\hbar = 1$, reads

$$\mathcal{H} = \mathcal{H}_{\text{Weyl}} + \mathcal{H}_{\text{Imp.}} + \mathcal{H}_{\text{Hyb.}}, \tag{1}$$

where

$$\mathcal{H}_{\text{Weyl}} = \sum_{\mathbf{k}s} \psi^\dagger_{\mathbf{k}s} s[D(\tilde{k}^J_- \sigma_+ + \tilde{k}^J_+ \sigma_-) + v_F(k_z - sQ)\sigma_z]\psi_{\mathbf{k}s} \tag{2}$$

is the part describing multi-Weyl fermions with spinor $\psi^\dagger_{\mathbf{k}s} = (c^\dagger_{\mathbf{k}s\uparrow} c^\dagger_{\mathbf{k}s\downarrow})$, $c^\dagger_{\mathbf{k}s\sigma}$ ($c_{\mathbf{k}s\sigma}$) for creation (annihilation) of an electron carrying winding number J, momentum $\mathbf{k}$, spin $\sigma = \uparrow, \downarrow$ and chirality $s = \pm 1$ for the Weyl nodes sQ, which break time-reversal symmetry. The nonrelativistic part is expressed in terms of $\tilde{k}_\pm = (k_x \pm ik_y)/k_D$, being $k_D = D/v_F$ (D) the *Debye-like* momentum (energy) cutoff as in graphene system [38], $\sigma_\pm = \frac{1}{2}(\sigma_x \pm i\sigma_y)$ and σ_z are the Pauli matrices. We stress that the winding number J, namely, the topological charge, gives the number of Fermi arcs pairs at the system boundaries, as ensured by the "bulk-boundary" correspondence principle [10]. In the last term of Eq. (2), which is of relativistic-type, the slope of the Dirac cones in the z direction of the momentum space is the Fermi velocity v_F.

The band-structure of Eq. (2) can be computed straightforwardly and leads to the following dispersion relation

$$\varepsilon^\pm_{\mathbf{k}s} = \pm v_F \sqrt{k^2_{zs} + |\tilde{k}_+|^{2J} k^2_D}, \tag{3}$$

wherein $+(-)$ corresponds to the conduction (valence) band, with $k_{zs} = k_z - sQ$ and it is depicted in Figs. 1(b)–1(d). Additionally, it is worth mentioning that for $J = 1$ (single Weyl) the Weyl semimetal has well-defined Dirac cones in all momentum directions [Fig. 1(b)], while for $J \gg 1$, we have a hypothetical hyper Weyl semimetal case [Fig. 1(d)], in which its band-structure shape saturates due to a huge topological charge. Further, a single Anderson-like impurity [32] can be described by the Hamiltonian

$$\mathcal{H}_{\text{Imp.}} = -\frac{U}{2} + \sum_\sigma \left(\varepsilon_{d\sigma} + \frac{U}{2}\right) n_{d\sigma} + \frac{U}{2}\left(\sum_\sigma n_{d\sigma} - 1\right)^2, \tag{4}$$

where the impurity electronic energy level is $\varepsilon_{d\sigma}$, with number operator $n_{d\sigma} = (n_{d\sigma})^2 = d^\dagger_\sigma d_\sigma$, being $d^\dagger_\sigma$ (d_σ) the corresponding creation (annihilation) operator and U is the Coulomb repulsion between two electrons with opposite spins ($\bar{\sigma} = -\sigma$). The hybridization term, which accounts for the host-impurity coupling, reads

$$\mathcal{H}_{\text{Hyb.}} = v \sum_\sigma (f^\dagger_{0\sigma} d_\sigma + \text{H.c.}), \tag{5}$$

where the field operator

$$f_{0\sigma} = \frac{1}{\sqrt{\mathcal{N}}} \sum_{\mathbf{k}s} c_{\mathbf{k}s\sigma} \tag{6}$$

describes the host site locally coupled to an embedded quantum impurity, with v being the impurity-host coupling strength and $\mathcal{N}$ the number of states delimited by k_D.

We would like to call attention to the following: by making the choice $\varepsilon_{d\sigma} = -U/2$, the second term of Eq. (4) disappears and the Hamiltonian $\mathcal{H}$ becomes invariant under the particle-hole transformation $c_{\mathbf{k}s\sigma} \to c^{\dagger}_{-\mathbf{k}s\sigma}$ and $d_{\sigma} \to -d^{\dagger}_{\sigma}$. This characterizes the particle-hole symmetric regime of the model, which will be employed without loss of generality, in order to determine the system bulk LDOS. Consequently, the LDOS profile exhibits mirror symmetry in the energy domain ε and the bulk Fano profile can be finally known.

III. LDOS AND FANO PROFILE

From the time Fourier transform of the retarded Green's function (GF)

$$\mathcal{G}_{\sigma} = -i\theta(t)\langle\{f_{0\sigma}(t), f^{\dagger}_{0\sigma}(0)\}\rangle_{\mathcal{H}}, \tag{7}$$

i.e., $\tilde{\mathcal{G}}_{\sigma}$, we verify the validity of the Dyson equation

$$\tilde{\mathcal{G}}_{\sigma} = \tilde{\mathcal{G}}^{0}_{\sigma} + \tilde{\mathcal{G}}^{0}_{\sigma} v \tilde{\mathcal{G}}_{\mathrm{Imp}.\sigma} v \tilde{\mathcal{G}}^{0}_{\sigma} \tag{8}$$

via the equation-of-motion approach [39], with $\mathcal{G}^{0}_{\sigma}$ and

$$\mathcal{G}_{\mathrm{Imp}.\sigma} = -i\theta(t)\langle\{d_{\sigma}(t), d^{\dagger}_{\sigma}(0)\}\rangle_{\mathcal{H}} \tag{9}$$

representing the pristine multi-Weyl and impurity GFs, respectively. Thus the Fano formula [25,26] in the bulk

$$\mathrm{LDOS} = -\frac{1}{\pi}\mathrm{Im}\tilde{\mathcal{G}}_{\sigma} \tag{10}$$

is expected to emerge, if in the impurity

$$\mathrm{DOS} = -\frac{1}{\pi}\mathrm{Im}\tilde{\mathcal{G}}_{\mathrm{Imp}.\sigma}, \tag{11}$$

their resonant states [39] exhibit a lorentzian profile.

As we consider the case of $T \ll T_{\mathrm{K}} \to 0$ (Kondo temperature) [40] and the system has a pseudogap at the Fermi level, Kondo correlations do not emerge [14] and consequently, the Coulomb blockade regime [39] takes place. The latter is characterized solely by the resonant states $\varepsilon_{d\sigma}$ and $\varepsilon_{d\sigma} + U$, and the correlation U in $\tilde{\mathcal{G}}_{\mathrm{Imp}.\sigma}$, can be safely treated in the framework of the Hubbard-I approximation [7,8,39]. The Hubbard-I approximation is indeed, a mean-field calculation, i.e., a truncation scheme on the system GFs, which determines the impurity GF $\tilde{\mathcal{G}}_{\mathrm{Imp}.\sigma}$, in particular, by accounting for the electronic correlation U in Eq. (4) within a certain regime of validity. We stress that the presence of the Hubbard term U in Eq. (4), which shows a quadratic dependence on the number operator $n_{d\sigma}$, prevents inevitably, the analytical and exact evaluation of $\tilde{\mathcal{G}}_{\mathrm{Imp}.\sigma}$. This lack of completeness, naturally, does not catch the complete low-energy regime of the single impurity Anderson model [32]. More specifically, the one characterized by $T \ll T_{\mathrm{K}}$, $\varepsilon_{d\sigma} < 0$, $\varepsilon_{d\sigma} + U > 0$ and, as a result, the Kondo peak present in Eq. (11). We call the attention that such a resonance is a many-body effect, which is due to a spin-flip process between the electrons from the impurity and the host conduction states.

It is worth mentioning that one of us in Ref. [14] has demonstrated, by employing the numerical renormalization group [14], that the Kondo peak emerges solely in multi-Weyl semimetals when the Fermi level is off resonance from the Dirac point, i.e., the so-called charge neutrality point $\varepsilon = 0$. By approaching this spot, the multi-Weyl semimetal presents a pseudogap, as we will verify later on, that scales with the power law $(\varepsilon^2)^{1/J}$ in the topological charge J for the pristine host density of states. It means that at the charge neutrality point, the host does not contain states to screen in an antiferromagnetic way the localized magnetic moment at the impurity site and lead to the Kondo peak in the impurity density of states of Eq. (11). Thus the spin-flip process quenches and even with $T \ll T_{\mathrm{K}} \to 0$, for multi-Weyl semimetals, the Kondo peak does not rise at $\varepsilon = 0$. This scenario is fully distinct from a metallic system, once at the corresponding charge neutrality point, the pristine host density of states is finite. As the Hubbard-I method disregards such a spin-flip mechanism to obtain the impurity GF $\tilde{\mathcal{G}}_{\mathrm{Imp}.\sigma}$, then we can safely adopt it to our system, only if we maintain the Fermi level at $\varepsilon = 0$, where for multi-Weyl semimetals the absence of states is ensured. By taking into account such an assumption, we employ the well-established GF in the Hubbard-I approximation as follows:

$$\tilde{\mathcal{G}}_{\mathrm{Imp}.\sigma} = -\frac{1}{v^2\mathrm{Im}\tilde{\mathcal{G}}^{0}_{\sigma}}\left(\frac{w_x}{x+i} + \frac{w_{\bar{x}}}{\bar{x}+i}\right). \tag{12}$$

This ensures, as expected, the lorentzian line shape in the DOS, with $w_x = 1 - \langle n_{d\bar{\sigma}}\rangle$ and $w_{\bar{x}} = 1 - w_x$ being spectral weights for the dimensionless resonant energies detuning

$$x = \frac{\varepsilon - \varepsilon_{d\sigma} - v^2\mathrm{Re}\tilde{\mathcal{G}}^{0}_{\sigma}}{-v^2\mathrm{Im}\tilde{\mathcal{G}}^{0}_{\sigma}} \tag{13}$$

and

$$\bar{x} = \frac{\varepsilon - \varepsilon_{d\sigma} - U - v^2\mathrm{Re}\tilde{\mathcal{G}}^{0}_{\sigma}}{-v^2\mathrm{Im}\tilde{\mathcal{G}}^{0}_{\sigma}}, \tag{14}$$

respectively, wherein

$$\langle n_{d\sigma}\rangle = \int_{-D}^{0} \mathrm{DOS} d\varepsilon \tag{15}$$

is the impurity occupation. The pristine host GF, or simply the propagator of the pristine Weyl fermions, is just

$$\begin{aligned}\tilde{\mathcal{G}}^{0}_{\sigma} &= \frac{1}{\mathcal{N}}\sum_{\mathbf{k}s}\frac{\varepsilon + i0^{+}}{(\varepsilon + i0^{+})^2 + (\varepsilon^{+}_{\mathbf{k}s})^2} = \mathrm{Re}\tilde{\mathcal{G}}^{0}_{\sigma} + i\mathrm{Im}\tilde{\mathcal{G}}^{0}_{\sigma} \\ &= \left|\tilde{\mathcal{G}}^{0}_{\sigma}\right|\exp(i\delta_J),\end{aligned} \tag{16}$$

where δ_J represents the phase of the propagator, in particular in the absence of the impurity, which is expected to depend upon the topological charge J via the dispersion relation $\varepsilon^{+}_{\mathbf{k}s}$ of Eq. (3). It reads

$$\tan\delta_J = \frac{\mathrm{Im}\tilde{\mathcal{G}}^{0}_{\sigma}}{\mathrm{Re}\tilde{\mathcal{G}}^{0}_{\sigma}}. \tag{17}$$

This quantity, as we will see later on, is deeply connected to the Fano asymmetry parameter q_J of the system, responsible for modulating the bulk Fano profile for the LDOS. Particularly for a multi-Weyl semimetal with $J \geqslant 3$, in addition, we will show that q_J becomes ruled by the angle $(360^{\circ}/2J)$, which surprisingly, is recognized as the angle of the rotational symmetry group C_{2J}. As we know, such a symmetry group stabilizes locally multi-Weyl points in the momentum space [15].

Now we are able to express the LDOS according to Fano formula [25,26]. We begin by introducing into Eq. (8), the quantities as follows:

$$\begin{aligned}\mathrm{Re}\tilde{\mathcal{G}}^0_\sigma &= -\frac{1}{\pi}\int_{-D}^{+D}\frac{\mathrm{Im}\tilde{\mathcal{G}}^0_\sigma}{\varepsilon - y}dy \\ &= -\frac{1}{\pi}\mathrm{sgn}(\varepsilon)\mathrm{Im}\tilde{\mathcal{G}}^0_\sigma\int_{-D/\varepsilon}^{+D/\varepsilon}\frac{(u^2)^{1/J}}{1-u}du \\ &= -q_J\mathrm{Im}\tilde{\mathcal{G}}^0_\sigma, \end{aligned} \tag{18}$$

due to the Kramers-Kronig relations [39], wherein $y = u\varepsilon$ and the Fano asymmetry parameter is given by

$$\begin{aligned} q_J &= -\frac{\mathrm{Re}\tilde{\mathcal{G}}^0_\sigma}{\mathrm{Im}\tilde{\mathcal{G}}^0_\sigma} = -\cot\delta_J, \\ &= \frac{1}{\pi}\mathrm{sgn}(\varepsilon)\mathrm{P.V.}\int_{-D/\varepsilon}^{+D/\varepsilon}\frac{(u^2)^{1/J}}{1-u}du, \end{aligned} \tag{19}$$

where P.V. stands for the Cauchy principal value and we clearly see that the phase δ_J of Eq. (17) for the pristine Weyl fermions propagator of Eq. (16) then dictates the Fano asymmetry parameter. Moreover,

$$\mathrm{Im}\tilde{\mathcal{G}}^0_\sigma = -\frac{3\pi^{3/2}\Gamma\left(\frac{1}{J}\right)}{2JD^{\frac{J+2}{J}}\Gamma\left(\frac{2+J}{2J}\right)}(\varepsilon^2)^{1/J}, \tag{20}$$

with $\Gamma(x)$ being the Gamma function and the power-law $(\varepsilon^2)^{1/J}$ is characterized by a pseudogap at the Fermi level ($\varepsilon = 0$).

We emphasize that Eq. (20) holds for arbitrary J and mention that so far, solely analytical expressions up to $J = 3$ were obtained [19]. We are aware that the crystalline rotational symmetry C_{2J} imposes the limitation $J \leqslant 3$, in particular when the spin degree of freedom comes into play [15]. However, the $J = 4$ case is still possible and emerges in spinless systems [36,37]. Thus we develop an extrapolation given by Eq. (20) and get a generalized Fano asymmetry parameter.

The aforementioned accomplishment was possible after employing in Eq. (16) the procedures as follows: (i) the standard substitution $\mathcal{N} = \sum_{\mathbf{k}s} \to \frac{\Omega}{(2\pi)^3}\int d^3\mathbf{k} = \frac{\Omega}{6\pi^2}k_D^3$, with Ω as the volume element in real space; and (ii) the hyperspherical transformation given by $k_x = k_D(\frac{\varepsilon^+_{\mathbf{k}s}\sin\theta}{D})^{\frac{1}{J}}\cos\phi$, $k_y = k_D(\frac{\varepsilon^+_{\mathbf{k}s}\sin\theta}{D})^{\frac{1}{J}}\sin\phi$ and $k_{zs} = k_D\frac{\varepsilon^+_{\mathbf{k}s}}{D}\cos\theta$ ($0 \leqslant \theta \leqslant \pi$, $0 \leqslant \phi \leqslant 2\pi$), with Jacobian

$$\mathrm{J}(\varepsilon^+_{\mathbf{k}s},\theta,\phi) = \frac{k_D^3}{D}\left(\frac{\varepsilon^+_{\mathbf{k}s}}{D}\right)^{2/J}\frac{(\sin\theta)^{\frac{2}{J}-1}}{J} \tag{21}$$

and property $\int\tilde{\mathcal{G}}^0_\sigma d^3\mathbf{k} = \int\tilde{\mathcal{G}}^0_\sigma\mathrm{J}(\varepsilon^+_{\mathbf{k}s},\theta,\phi)d\varepsilon^+_{\mathbf{k}s}d\theta d\phi$.

We can finally obtain the bulk Fano profile, which from here, we call by natural Fano profile (NFP), once it is expressed in terms of their natural coordinates x and $\bar{x}$. Taking into account the spin degree of freedom, we find the NFP=2LDOS$/\rho_0(1+q_J^2)$, with

$$\rho_0 = -\frac{1}{\pi}\mathrm{Im}\tilde{\mathcal{G}}^0_\sigma \tag{22}$$

as the pristine multi-Weyl DOS and

$$\mathrm{NFP} = \frac{2}{1+q_J^2}\left[w_x\frac{(x+q_J)^2}{x^2+1} + w_{\bar{x}}\frac{(\bar{x}+q_J)^2}{\bar{x}^2+1}\right], \tag{23}$$

which holds in the wide-band limit $D/\varepsilon \to \infty$. As we are interested in impurity levels nearby the Fermi energy, such a limit prevents that the time-reversal symmetry breaking lifts the system spin degeneracy [14]. From Eq. (23) and for $\varepsilon < 0$ ($\varepsilon > 0$), the NFP shows amplitudes of minimum and maximum at $x = -q_J$ ($\bar{x} = -q_J$) and $x = 1/q_J$ ($\bar{x} = 1/q_J$), respectively.

We highlight that the LDOS spectral line shape itself, as we shall see in the numerical analysis, will not exhibit a Fano profile as a function of energy ε for a given q_J, as it occurs for flat band systems with energy and J independent host DOS [33–35]. Additionally, we will verify that for the revealing of such a behavior, one should analyze the Fano profile as a function of x or $\bar{x}$, namely, the natural coordinates for the Fano profile to emerge. Nevertheless, before that, we should firstly evaluate carefully the integral over u variable in Eq. (19).

We call attention that, in particular for $q_{J=1}$ and $q_{J=2}$, the functions depending on u do not vanish in the limits $u \to \pm\infty$, which is a common pathology in low-energy models [38]. This feature constitutes a technical difficulty in solving Eq. (19) numerically. Hence, to handle accordingly with this lack of integrability issue, we should, as already performed in graphene system [38], solve first the integral analytically by keeping the ratio D/ε finite and assuming later on, the limit $\varepsilon/D \ll 1$ in the $\mathrm{Re}\tilde{\mathcal{G}}_{\sigma^0}$ evaluations. Such cases are then described by

$$\mathrm{Re}\tilde{\mathcal{G}}^0_\sigma(J=1) = \frac{3\varepsilon}{D^3}\left(\varepsilon\ln\frac{|D+\varepsilon|}{|D-\varepsilon|} - 2D\right) \tag{24}$$

and

$$\mathrm{Re}\tilde{\mathcal{G}}^0_\sigma(J=2) = \frac{3\pi}{4D^2}\varepsilon\ln\frac{\varepsilon^2}{|\varepsilon^2 - D^2|}, \tag{25}$$

respectively, which provide

$$q_{J\leqslant 2} = -\frac{\mathrm{Re}\tilde{\mathcal{G}}^0_\sigma(J\leqslant 2)}{\mathrm{Im}\tilde{\mathcal{G}}^0_\sigma(J\leqslant 2)} = -\cot\delta_{J\leqslant 2} \tag{26}$$

as dependent both on energy for $\varepsilon/D \ll 1$ and topological charge J.

However, the necessary vanishing behavior is present in $q_{J\geqslant 3}$ as a function of u and consequently, it makes the integral in Eq. (19) to behave finite for $D/\varepsilon \to \infty$, which can be found analytically simultaneously with the ratio $D/\varepsilon \to \infty$. This results into an interesting finding, i.e., an energy-independent Fano asymmetry parameter discretized in the topological charge J, which reads

$$q_{J\geqslant 3} = -\mathrm{sgn}(\varepsilon)\tan(C_{2J\geqslant 6}), \tag{27}$$

where we define $C_{2J} \equiv (360^\circ/2J)$ as the angle for the corresponding rotational symmetry group. Together with Eqs. (24)–(26), this gives the set of analytical expressions that defines the topological charge Fano effect in multi-Weyl

systems. Notice that for $J = 3$, $q_{J=3} = -\mathrm{sgn}(\varepsilon)\tan(C_{2J=6}) = -\mathrm{sgn}(\varepsilon)\sqrt{3}$, while for $J \gg 1$, we have $|q_{J\gg1}| \to 0$, which corresponds to the maximum allowed point group symmetry protected case, namely, the $C_{2J=6}$ rotational symmetry group, and the hypothetical hyper Weyl semimetal, respectively.

We emphasize that for $J \leqslant 3$ such a crystalline symmetry, hereby expressed in Eq. (27) via the C_{2J} parameter, then stabilizes the merge of chiral-degenerate Weyl points with $J = 1$ each and leads to an unique point enclosing a multitopological charge $J > 1$. This spot in momentum space is the so-called multi-Weyl point, where the aforementioned symmetry glues together multiple Weyl points with unitary topological charge and prevent them to split away.

Thus we can point out that the Fano parameter role in the accounted picture is self-contained in Eq. (27) and arises from Eq. (17), which authorizes the link $q_{J\geqslant3} = -\cot\delta_{J\geqslant3} = -\mathrm{sgn}(\varepsilon)\tan(C_{2J\geqslant6})$, from where we perceive that the NFP of Eq. (23) becomes settled by the topological charge J. As for $J \geqslant 3$ the phase $\delta_{J\geqslant3}$ of the Weyl fermions in the propagator of Eq. (16) depends on the dispersion relation $\varepsilon^{+}_{\mathbf{k}s}$ of Eq. (3), it yields the Fano asymmetry parameter $q_{J\geqslant3}$ to be ruled by the angle $(360^\circ/2J)$, which is related to the rotational symmetry group $C_{2J\geqslant6}$. Distinctly, for $J \leqslant 2$ the dispersion relation $\varepsilon^{+}_{\mathbf{k}s}$ introduces in $q_{J\leqslant2}$ of Eq. (26) complex dependencies on the topological charge J, in particular obeying Eqs. (24) and (25), which affect peculiarly the NFP of Eq. (23).

As aftermath, independently of the J strength, the broadening of the impurity levels [Eq. (12)] and the LDOS change into a Fano-type profile in the natural coordinates [Eq. (23)], are expected to occur in both the scenarios. In summary, the system exhibits two paths of transport that interfere to each other: one consists of electrons that travel through the orbital $f_{0\sigma}$ of the host and that wherein they visit the impurity d_σ and return to $f_{0\sigma}$, being a process modulated by q_J.

IV. RESULTS AND DISCUSSION

A. Natural Fano profile and discretized Fano parameter

As stated previously, we consider the particle-hole symmetric regime. In this case, $\varepsilon_{d\sigma} = -U/2$ and $w_x = w_{\bar{x}} = 1/2$ ($\langle n_{d\bar{\sigma}}\rangle = 1/2$ from self-consistent calculations), with $U = v = 0.14D$. Taking into account Eq. (23), in Fig. 2, we present the spectral analysis of the bulk LDOS $= \rho_0\frac{(1+q_J^2)}{2}$NFP as a function of ε and the first part of the NFP versus x for several J values. As the dimensionless resonant energy detuning x is proportional to the deviation from the resonant state $\varepsilon_{d\sigma} = -U/2$ within the valence band, its domain holds for $\varepsilon < 0$. Thus the second part of Eq. (23) as a function of $\bar{x}$ exhibits a reversed profile, once $\bar{x} = -x$ in the domain $\varepsilon > 0$ (conduction band), where the resonant state $\varepsilon_{d\sigma} + U = U/2$ resides and $\mathrm{Re}\tilde{\mathcal{G}}^0_\sigma(\varepsilon > 0) = -\mathrm{Re}\tilde{\mathcal{G}}^0_\sigma(\varepsilon < 0)$ fulfills particle-hole symmetry [14]. Hence, the dependence of Eq. (23) on $\bar{x}$ is not shown, for a sake of simplicity.

Counterintuitively, the LDOS in Fig. 2(a) does not show Fano profiles around the resonant states as a function of ε upon changing J, as it should occur, despite the Fano parameters being dictated by Eqs. (26) and (27). Such a feature arises from the topological charge J and energy ε dependencies present in the resonant states broadening $\Delta = -2v^2\mathrm{Im}\tilde{\mathcal{G}}_{\sigma^0} =$

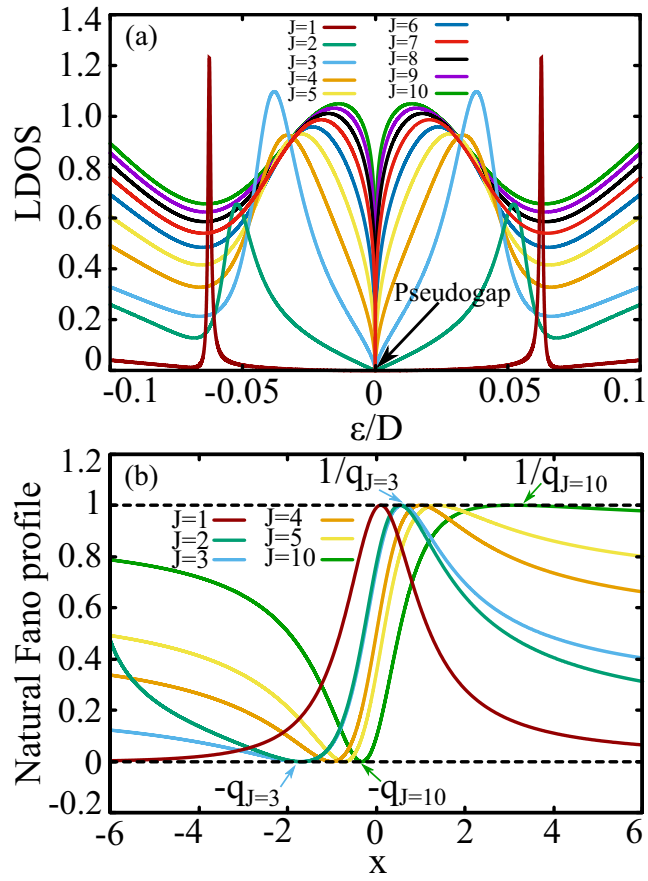

FIG. 2. (a) LDOS $= \rho_0\frac{(1+q_J^2)}{2}$NFP [Eq. (23)] versus energy ε in units of the cutoff D for several J values and particle-hole symmetric regime: $\varepsilon_{d\sigma} = -U/2$ and $w_x = w_{\bar{x}} = 1/2$, with $U = v = 0.14D$ (see the main text). The increase of J turns the pseudogap flanked by the impurity resonant states more pronounced with a sharp dip. (b) Natural Fano profile NFP [first part of Eq. (23)] vs x and dependent on J for $\varepsilon < 0$. In the case of $\varepsilon > 0$, the profile is just reversed as a function of $\bar{x}$ and it is not shown, for a sake of simplicity. We clearly verify that J modulates the Natural Fano profile.

$2\pi v^2\rho_0$ and quasiparticle dressing term $v^2\mathrm{Re}\tilde{\mathcal{G}}^0_\sigma$ of the impurity. These quantities, in particular, appear in the resonant energies detuning $x = 2(\varepsilon - \varepsilon_{d\sigma} - v^2\mathrm{Re}\tilde{\mathcal{G}}^0_\sigma)/\Delta$ and $\bar{x} = 2(\varepsilon - \varepsilon_{d\sigma} - U - v^2\mathrm{Re}\tilde{\mathcal{G}}^0_\sigma)/\Delta$ entering into Eq. (23). From the latter, we perceive that x and $\bar{x}$ are not linearly proportional to ε. This characteristic is restored when Δ and $v^2\mathrm{Re}\tilde{\mathcal{G}}^0_\sigma$ become energy and J independent, as verified in metallic flat bands near the Fermi level [33–35]. Consequently, solely in this particular situation, the LDOS profile as a function of ε shows Fano line shapes.

Therefore, in the case of multi-Weyl semimetals, one should analyze $2\mathrm{LDOS}/\rho_0(1+q_J^2)$, namely, the NFP given by Eq. (23), as a function of the natural coordinate x or $\bar{x}$ instead of ε, to indeed perceive the emerging NFP around $x = 0$ or $\bar{x} = 0$. Such analysis appears in Fig. 2(b), where we verify that the increase of J drives the system from the resonant Fano profile for the case of single Weyl semimetal $J = 1$, towards the hyper Weyl semimetal with $J \gg 1$, which is identified by an antiresonant line shape. Further, the Fano

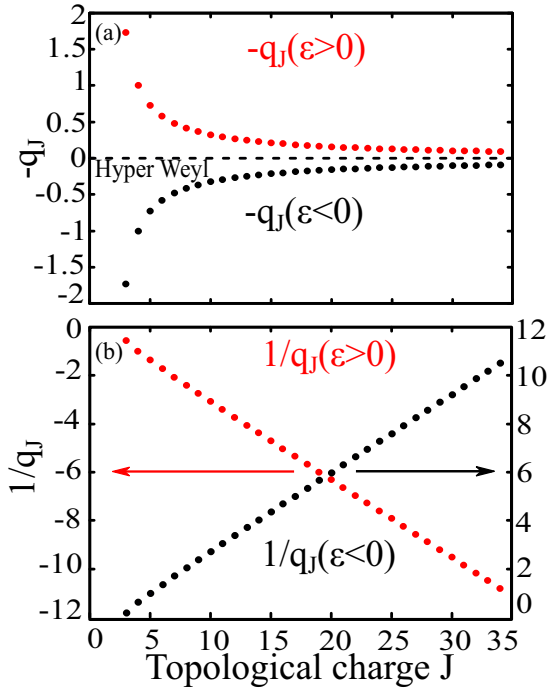

FIG. 3. (a) Minimum amplitude position $-q_J$ of the Fano profile from Eq. (27) [see also Figs. 1(c) and 2(b)] with decaying behavior as a function of $J \geqslant 3$ for energies $\varepsilon > 0$ and $\varepsilon < 0$. (b) The same for the maximum amplitude position $1/q_J$, but with a linear dependence on J. (a) and (b) make explicit that the Fano asymmetry parameter q_J given by Eq. (27) consists of a discretized quantity in the J term, yielding the topological charge Fano effect.

minimum and maximum amplitudes positions for $\varepsilon < 0$ given by $x = -q_J$ and $x = 1/q_J$, respectively, then appear in such a figure marked by arrows, just in order to make explicit the discretized Fano parameter in J. However, in Fig. 2(a) for the LDOS representation as a function of ε, the role of J solely lies in the renormalization of the resonant states towards the Fermi level as J increases, pointing out that the semimetallic pseudogap becomes characterized by an extremely sharp dip, due to its spectral power-law $(\varepsilon^2)^{1/J}$ in Eq. (20).

It is worth noting that the discretization observed in Fig. 2(b) arises from Eq. (27), which together with Eqs. (24)–(26) are the most capital ones of the current work: they encode the topological charge Fano effect in multi-Weyl systems, once they allow the tuning of the Fano line shape by changing the topological charge J. Equivalently, according to the "bulk-boundary" correspondence, the pairs of Fermi arcs surface states present at the system boundaries are fixed by the J value [10], which also imposes the Fano profile line shape of the bulk.

With this in mind, we see from Fig. 3(a) that for $\varepsilon < 0$ the limits $-q_{J\to 3} \to -\tan(C_{2J=6}) = -\sqrt{3}$ and $-q_{J\gg 1} \to 0$ are reached, while for $\varepsilon > 0$ we have $-q_{J\to 3} \to \tan(C_{2J=6}) = \sqrt{3}$ and $-q_{J\gg 1} \to 0$. Interestingly enough for $J = 3$, $|q_{J=3}| = \tan(C_{2J=6}) = \sqrt{3} \approx 1,732$ and the Fano profile, according to Fig. 2(b), rises as asymmetric. Particularly for the $-q_J$ decaying behavior with J reported in Fig. 3(a), we highlight that such a feature is connected straightforwardly to the system band structure. As stated previously, the band-structure saturates into one characteristic for the hyper Weyl semimetal-type with $J \gg 1$, as depicted in Fig. 1(d). As an aftermath, if the shape generated by the dispersion $\varepsilon^{\pm}_{\mathbf{k}s}$ from Eq. (3) remains unchanged by increasing $J \gg 1$ [Fig. 1(d)], so does the Fano parameter, which attains to $|q_{J\gg 1}| \to 0$, once it depends on $\varepsilon^{+}_{\mathbf{k}s}$ via the GF $\tilde{\mathcal{G}}^0_\sigma$ of the pristine host. As a result, the antiresonant Fano profile becomes the hallmark of hyper Weyl semimetals.

In Fig. 3(b), we show the corresponding behavior for $1/q_J$, which is linear instead. Note that $1/q_J$ for $\varepsilon < 0$ follows an increasing linear trend, while for $\varepsilon > 0$ it is the opposite. This reflects the own particle-hole symmetry characteristic of the Fano parameter and it occurs because the multi-Weyl points and Fermi level are energy-degenerate. Thereby, the band-structure also has particle-hole symmetry, as well as the $1/q_J$ quantity. Most importantly, both the $-q_J$ and $1/q_J$ behaviors as functions of J make explicit that the Fano parameter is discretized, thus characterizing the topological charge Fano effect in multi-Weyl semimetals.

B. Experimental proposal to detect the topological charge Fano effect

From the spectral analysis performed so far, we perceive that the NFP of Eq. (23) requires natural coordinates to be viewed, such as x and $\bar{x}$ from Eqs. (13) and (14), respectively. This characteristic relies in the fact that both the latter expressions are highly nonlinear functions in the ε degree, which turns the detection of the Fano profiles encoded by Eq. (23) a hard challenge by varying ε. However, we propose an alternative path to overcome such an experimental obstacle. We begin with by noticing that if we consider the impurity level $\varepsilon_{d\sigma} = \varepsilon_d$ in Eq. (4) a tunable parameter, while ε, $\mathrm{Re}\tilde{\mathcal{G}}^0_\sigma$ and $\mathrm{Im}\tilde{\mathcal{G}}^0_\sigma$ as constant numbers, we finally gain the desired linear dependence of x and $\bar{x}$, not with ε, but with ε_d instead. Thus Eq. (23) as a function of ε_d is expected to show Fano profiles, once ε_d rises as the natural coordinate for the emanation of the Fano profile. The tunability of ε_d to become feasible from an experimental perspective needs a remake of Fig. 1(a) into the transport-type device of Fig. 4(a), which we introduce as the multi-Weyl bar.

The multi-Weyl bar consists of a quasilinear bulk system with an external impurity, where this side-coupled impurity is supposed to overlap with both the surface and bulk states of the system. A similar approach was done to the electron channel treated in the quantum wire theoretically explored in Ref. [41]. In such a work, one of us derived a transmittance formula of an impurity side-coupled to the electron channel and found Fano profiles in the zero-bias conductance by tuning ε_d, due to the assumption of a gate voltage V_g attached to this impurity. It was found that the conductance reflects the system bulk properties via the transmittance coefficient, hereby with the shorthand notation $\mathcal{T}_{\mathrm{Bulk}}(\varepsilon_d) = \mathcal{G}/\mathcal{G}_0$, where $\mathcal{G}$ is the zero-bias conductance at $T \ll T_{\mathrm{K}} \to 0$ and $\mathcal{G}_0 = e^2/h$ stands for the conductance quantum. The bulk properties come up, once $\mathcal{T}_{\mathrm{Bulk}}(\varepsilon_d)$ depends upon the spectral density of the host site described by the fermionic operator connected to the impurity. Thus, in our system, this corresponds to Eq. (6) for $f_{0\sigma}$ and consequently, it allows, together with Eq. (23) for the NFP and the quantum transport formalism developed in Ref. [41], to derive the equality $\mathcal{T}_{\mathrm{Bulk}}(\varepsilon_d) = \mathrm{NFP}$. As the NFP

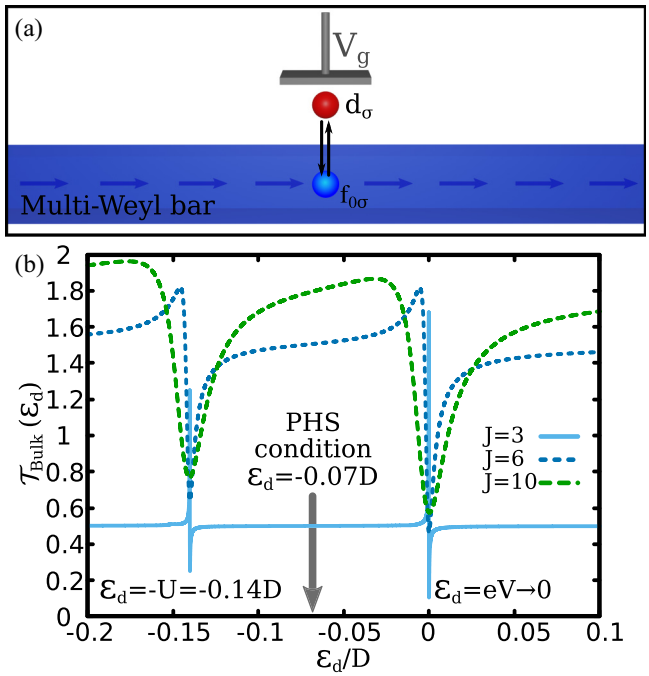

FIG. 4. (a) Sketch of the multi-Weyl bar device, where an impurity appears side-coupled. The arrows denote the current direction from the source to drain leads (not depicted). This system consists of an experimental proposal for detecting the topological charge Fano effect. (b) The bulk transmittance $\mathcal{T}_{\rm Bulk}(\varepsilon_d) = {\rm NFP}$ versus ε_d for several J values is determined via Eq. (23), with $\varepsilon = {\rm eV} \to 0$ as a small bias-voltage. The ε_d degree is tunable by a gate voltage V_g attached to the impurity, thus leading to a transmittance with Fano profiles nearby the energies $\varepsilon_d = -U$ and $\varepsilon_d = {\rm eV}$. Around them, we can apply Eq. (23) to experimental data, extract the Fano asymmetry parameter q_J and estimate via Eq. (27) the topological charge J. The middle point between such energy positions corresponds to the particle-hole symmetry (PHS), wherein the condition $\varepsilon_d = -U/2$ is fulfilled.

is bounded by 2, this upper limit represents the maximum of the transmittance by accounting for the two spin channels.

However, we should adapt carefully the transport formalism done in Ref. [41] for a quantum wire to multi-Weyl semimetals in the geometry of the bar depicted in Fig. 4(a). First, multi-Weyl semimetals have pseudogap [Eq. (20)] and it does not make sense to perform a zero-bias analysis, but this can be easily solved by placing $\mathcal{T}_{\rm Bulk}(\varepsilon_d)$ slightly off the charge neutrality point $\varepsilon = 0$, namely $\varepsilon = {\rm eV} \to 0$, being eV a small bias voltage in which the system conducts. This fixes ε, ${\rm Re}\tilde{\mathcal{G}}^0_\sigma$ and ${\rm Im}\tilde{\mathcal{G}}^0_\sigma$ at $eV \to 0$ in Eqs. (13) and (14) for x and $\bar{x}$, respectively, thus restoring the highly desired linearity of these quantities with ε_d, which is necessary for the Fano profiles to appear. Second, the practical realization of the multi-Weyl bar implies in a finite system, where the Fermi arcs surface states contribute inevitably to the total transmittance, together with the bulk states with eV $\to 0$. Despite this present characteristic of the experimental proposal, as Fermi arcs surface states are topologically protected [1–8], in opposite to the bulk states, the Fano patterns in the total transmittance as a function of ε_d are expected to have the latter as their source. This means that topologically protected states are supposed to stay robust under external perturbations, in particular, those that do not break the symmetry that protect such states. In this manner, these states become immune to Fano interference. Here, by changing ε_d, the particle-hole symmetry (PHS) of the Hamiltonian of Eq. (1) breaks down, but it does not unprotec topologically the Fermi arcs surface states, once they are not protected by such a symmetry. Consequently, the Fano patterns in the total transmittance are expected to be dictated by $\mathcal{T}_{\rm Bulk}(\varepsilon_d)$, which for $\varepsilon = {\rm eV} \to 0$, leads to Fano profiles around $\varepsilon_d = -U$ and $\varepsilon_d = {\rm eV}$, as shown in Fig. 4(b) for several J values.

We stress that the quantification concerning whether the total transmittance depends weakly on the Fermi arcs surface states is not the focus of the main analysis of the current work. Thus further investigation into the dependence degree of the Fano interference on the Fermi arcs surface states will be addressed elsewhere. It is worth emphasizing that the proposed device depicted in Fig. 4(a) points out a way to induce Fano line shapes in the total transmittance, just by changing ε_d for fixed small bias-voltage eV $\to 0$. Experimentally speaking, from one detected Fano line shape, we can extract the Fano asymmetry parameter q_J via Eq. (23) and by employing Eq. (27), for instance, determine the topological charge J.

To summarize, for $\mathcal{T}_{\rm Bulk}(\varepsilon_d)$ versus ε_d, the Fano line shape in Fig. 4(b) is also modulated by J and obeys the same trend previously observed in Fig. 2(b). Equivalently, the deeper meaning of the "bulk-boundary" correspondence applied to the here proposed Fano effect is the following: the greater the amount of Fermi arcs surface states given by J at the system boundaries, the more the Fano profile will be antiresonant within the bulk.

V. CONCLUSIONS

In this work, we determine the Fano asymmetry parameter for a single impurity coupled to a multi-Weyl semimetal and introduce the concept of topological charge Fano effect. According to the "bulk-boundary" correspondence, which states that the number of Fermi arcs at the boundaries of a finite size system is determined by the magnitude of the topological charge, known from its bulk version with infinite size, we then reveal the modulation of the system Fano profile, due to the bulk LDOS, by such surface states. This can be emulated in our theoretical framework by the tuning of the topological charge value, which allows the Fano profile to change from the resonant pattern for single Weyl semimetal, towards the antiresonant Fano line shape, which identifies hyper Weyl semimetals. Additionally, for the maximum allowed protected case by the rotational symmetry group $C_{2J=6}$, namely, the triple Weyl semimetal $J = 3$ and rotational angle defined by $C_{2J} \equiv (360^\circ/2J)$, we predict the absolute Fano parameter $|q_{J=3}| = \tan(C_{2J=6})$ and an asymmetric Fano profile. Additionally, we indicate a quantum transport setup where we expect that the here proposed Fano effect could be present.

ACKNOWLEDGMENTS

We thank the Brazilian funding agencies CNPq (Grants No. 302887/2020-2, No. 308410/2018-1, No. 311980/2021-0, No. 305738/2018-6, No. 311366/2021-0, No. 305668/2018-8,

and No. 308695/2021-6), Coordenação de Aperfeiçoamento de Pessoal de Nível Superior–Brasil (CAPES) – Finance Code 001, the São Paulo Research Foundation (FAPESP; Grant No. 2018/09413-0) and FAPERJ Process No. 210 355/2018. L.S.R. and I.A.S. acknowledge support from the Icelandic Research Fund (project "Hybrid polaritonics"). I.A.S. also acknowledges support from the Program Priority 2030. L.S.R. thanks A.C.S. and Unesp for their hospitality.

[1] M. Z. Hasan, G. Chang, I. Belopolski, G. Bian, S.-Y. Xu, and J.-X. Yin, Nat. Rev. Mater. **6**, 784 (2021).
[2] M. Z. Hasan, S.-Y. Xu, I. Belopolski, and S.-M. Huang, Annu. Rev. Condens. Matter Phys. **8**, 289 (2017).
[3] B. Yan and C. Felser, Annu. Rev. Condens. Matter Phys. **8**, 337 (2017).
[4] H. Zheng and M. Zahid Hasan, Adv. Phys.: X **3**, 1466661 (2018).
[5] N. P. Armitage, E. J. Mele, and A. Vishwanath, Rev. Mod. Phys. **90**, 015001 (2018).
[6] J. Hu, S.-Y. Xu, N. Ni, and Z. Mao, Annu. Rev. Mater. Res. **49**, 207 (2019).
[7] Y. Marques, W. N. Mizobata, R. S. Oliveira, M. de Souza, M. S. Figueira, I. A. Shelykh, and A. C. Seridonio, Sci. Rep. **9**, 8452 (2019).
[8] W. N. Mizobata, Y. Marques, M. Penha, J. E. Sanches, L. S. Ricco, M. de Souza, I. A. Shelykh, and A. C. Seridonio, Phys. Rev. B **102**, 075120 (2020).
[9] S. Park, S. Woo, E. J. Mele, and H. Min, Phys. Rev. B **95**, 161113(R) (2017).
[10] R. M. A. Dantas, F. Peña-Benitez, B. Roy, and P. Surówka, Phys. Rev. Research **2**, 013007 (2020).
[11] T. Hayata, Y. Kikuchi, and Y. Tanizaki, Phys. Rev. B **96**, 085112 (2017).
[12] G. Xu, H. Weng, Z. Wang, X. Dai, and Z. Fang, Phys. Rev. Lett. **107**, 186806 (2011).
[13] Q. Liu and A. Zunger, Phys. Rev. X **7**, 021019 (2017).
[14] G. T. D. Pedrosa, J. F. Silva, and E. Vernek, Phys. Rev. B **103**, 045137 (2021).
[15] C. Fang, M. J. Gilbert, X. Dai, and B. A. Bernevig, Phys. Rev. Lett. **108**, 266802 (2012).
[16] R. M. A. Dantas, F. Peña-Benitez, B. Roy, and P. Surówka, J. High Energy Phys. 12 (2018) 069.
[17] S. Ahn, E. J. Mele, and H. Min, Phys. Rev. B **95**, 161112(R) (2017).
[18] S. P. Mukherjee and J. P. Carbotte, Phys. Rev. B **97**, 045150 (2018).
[19] H.-F. Lü, Y.-H. Deng, S.-S. Ke, Y. Guo, and H.-W. Zhang, Phys. Rev. B **99**, 115109 (2019).
[20] Q. Chen and G. A. Fiete, Phys. Rev. B **93**, 155125 (2016).
[21] T. Nag and S. Nandy, J. Phys.: Condens. Matter **33**, 075504 (2020).
[22] B. Sadhukhan and T. Nag, arXiv:2203.12756.
[23] A. H. Castro Neto, F. Guinea, N. M. R. Peres, K. S. Novoselov, and A. K. Geim, Rev. Mod. Phys. **81**, 109 (2009).
[24] S.-M. Huang, S.-Y. Xu, I. Belopolski, C.-C. Lee, G. Chang, T.-R. Chang, B. Wang, N. Alidoust, G. Bian, M. Neupane, D. Sanchez, H. Zheng, H.-T. Jeng, A. Bansil, T. Neupert, H. Lin, and M. Z. Hasan, Proc. Natl. Acad. Sci. USA **113**, 1180 (2016).
[25] U. Fano, Phys. Rev. **124**, 1866 (1961).
[26] A. E. Miroshnichenko, S. Flach, and Y. S. Kivshar, Rev. Mod. Phys. **82**, 2257 (2010).
[27] Y. S. Joe, A. M. Satanin, and C. S. Kim, Phys. Scr. **74**, 259 (2006).
[28] J. J. Xia, S. Q. Duan, and W. Zhang, Nanoscale Res. Lett. **10**, 223 (2015).
[29] L. S. Ricco, V. L. Campo, I. A. Shelykh, and A. C. Seridonio, Phys. Rev. B **98**, 075142 (2018).
[30] M. F. Limonov, M. V. Rybin, A. N. Poddubny, and Y. Kivshar, Nat. Photon. **11**, 543 (2017).
[31] J. Gollwitzer, L. Bocklage, R. Röhlsberger, and G. Meier, npj Quantum Inf. **7**, 114 (2021).
[32] P. W. Anderson, Phys. Rev. **124**, 41 (1961).
[33] V. Madhavan, W. Chen, T. Jamneala, M. Crommie, and N. Wingreen, Science **280**, 567 (1998).
[34] N. Knorr, M. A. Schneider, L. Diekhöner, P. Wahl, and K. Kern, Phys. Rev. Lett. **88**, 096804 (2002).
[35] O. Újsághy, J. Kroha, L. Szunyogh, and A. Zawadowski, Phys. Rev. Lett. **85**, 2557 (2000).
[36] C. Cui, X.-P. Li, D.-S. Ma, Z.-M. Yu, and Y. Yao, Phys. Rev. B **104**, 075115 (2021).
[37] T. Zhang, R. Takahashi, C. Fang, and S. Murakami, Phys. Rev. B **102**, 125148 (2020).
[38] B. Uchoa, V. N. Kotov, N. M. R. Peres, and A. H. Castro Neto, Phys. Rev. Lett. **101**, 026805 (2008).
[39] H. Bruus and K. Flensberg, *Many-Body Quantum Theory in Condensed Matter Physics, An Introduction* (Oxford University Press, Oxford, 2012).
[40] A. C. Hewson, *The Kondo Problem to Heavy Fermions* (Cambridge University Press, Cambridge, 1993).
[41] A. C. Seridonio, M. Yoshida, and L. N. Oliveira, Europhys. Lett. **86**, 67006 (2009).